LETTERS
https://doi.org/10.1038/s41566-019-0396-4

nature photonics

# Stimulated Raman excited fluorescence spectroscopy and imaging

Hanqing Xiong[1,2], Lixue Shi[1,2], Lu Wei[1], Yihui Shen[1], Rong Long[1], Zhilun Zhao[1] and Wei Min[1*]

**Powerful optical tools have revolutionized science and technology. The prevalent fluorescence detection offers superb sensitivity down to single molecules but lacks sufficient chemical information[1–3]. In contrast, Raman-based vibrational spectroscopy provides exquisite chemical specificity about molecular structure, dynamics and coupling, but is notoriously insensitive[3–5]. Here, we report a hybrid technique of stimulated Raman excited fluorescence (SREF) that integrates superb detection sensitivity and fine chemical specificity. Through stimulated Raman pumping to an intermediate vibrational eigenstate, followed by an upconversion to an electronic fluorescent state, SREF encodes vibrational resonance into the excitation spectrum of fluorescence emission. By harnessing the narrow vibrational linewidth, we demonstrated multiplexed SREF imaging in cells, breaking the 'colour barrier' of fluorescence. By leveraging the superb sensitivity of SREF, we achieved all-far-field single-molecule Raman spectroscopy and imaging without plasmonic enhancement, a long-sought-after goal in photonics. Thus, through merging Raman and fluorescence spectroscopy, SREF would be a valuable tool for chemistry and biology.**

To merge the advantages from both the worlds of Raman and fluorescence, our idea is to develop a new hybrid spectroscopy by encoding vibrational features onto the fluorescence spectrum. Before we reach the optimized design, we have gone through a series of theoretical considerations and experimental refinement (Fig. 1). Whereas linear fluorescence spectroscopy excites the electronic transition directly (Fig. 1a), nonlinear fluorescence excitation can employ one or more virtual states as intermediates, thus potentially probing more states (Fig. 1b). However, conventional nonlinear fluorescence still lacks chemical specificity, owing to the extremely short-lived virtual states (that is, large energy uncertainty). We reason that, if a long-lived vibrational eigenstate with a well-defined energy level can mediate a multiphoton fluorescence excitation process, the intermediate vibrational information can then be encoded into the fluorescence excitation spectrum. Indeed, such double-resonance spectroscopy was explored decades ago in which an infrared (IR) pulse excites an intermediate vibrational transition, followed by a visible pulse to excite the fluorescence (Fig. 1c)[6]. Despite being a powerful approach to investigate the vibrational dynamics of chromophores[7,8], the strong IR absorption in water and poor spatial resolution are intrinsically unfavourable for applications in biological systems. Moreover, the reported sensitivity is still several orders away from single molecules.

Considering stimulated Raman scattering (SRS) is complementary to IR excitation by offering much higher spatial resolution and avoiding water absorption, we take a different approach, stimulated Raman-excited fluorescence (SREF), by harnessing two beams (pump and Stokes) to coherently populate the intermediate vibrational state via SRS, and a third probe beam to up-convert the vibrational population to the electronic excited state for subsequent fluorescence (Fig. 1d). Unlike conventional fluorescence spectroscopy (Fig. 1a,b), SREF is a Raman-mediated three-photon process, thus its excitation spectrum, by tuning $\omega_p - \omega_s$, should map out the vibrational information of the electronic ground state. Figure 1e illustrates the microscope set-up (details in the Methods and Supplementary Fig. 1). Briefly, temporally and spatially overlapped pump ($\omega_p$, tunable) and Stokes ($\omega_s$, 1031.2 nm) picosecond pulse trains are focused by a high numerical aperture (NA) objective to perform SRS excitation. The pump pulse (either through one photon or two photons) also plays the role of a probe pulse (green line or red dashed line) for excitation to the electronic excited state for fluorescence emission. Backward fluorescence is then detected by a small-area avalanche photodiode (APD) with confocal detection. Both the reflected laser beams and the coherent anti-Stoke Raman scattering (CARS) signal[9] are completely blocked by appropriate filter sets.

However, our initial attempt on a coumarin dye (SRS excitation of C=C mode followed up by two-photon excitation to the fluorescent state) failed to detect any vibrational feature by tuning $\omega_p - \omega_s$. We found that, even with a quantum amplification up to $10^8$, achieved under modern SRS microscopy[10], the effective SRS excitation cross-sections are still less than $10^{-20}$ cm$^2$ for typical chromophores including coumarin, resulting in much less efficient vibrational pumping rate compared to the rapid vibrational relaxation (sub-picosecond) of molecules in condensed phases[7]. As a result, this SREF pathway is easily overwhelmed by other competing processes such as the two-photon fluorescence background, which was observed in our attempt on coumarin and a previous unsuccessful trial on perylene dye[11].

We note that the above unsuccessful SREF attempt should be associated with SRS being operated in the non-resonance region (Fig. 1d), with the pump laser energy, $\omega_p$, being well below the molecular absorption peak energy, $\omega_{abs}$. It is well known[12] that the Raman cross-section of electronically coupled vibrational modes can be enhanced up to $10^7$ when $\omega_p$ is brought close to $\omega_{abs}$. We then revisited the SREF approach, aiming to significantly enhance the SRS pumping rate under the close electronic resonance (Fig. 1f). A near-IR dye ATTO 740 ($\omega_{abs}$, 760 nm in dimethyl sulfoxide (DMSO)) and its nitrile mode (Raman peak at 2,227 cm$^{-1}$) was used in our second attempt (Supplementary Fig. 2a). The SREF excitation spectra of ATTO 740 were acquired by tuning $\omega_p$ across the nitrile Raman peak. Although a strong SRS peak was detected as stimulated Raman loss of the pump beam, no vibrational feature was observed on the fluorescence excitation spectrum. Apparently, a too close resonance condition of SRS is unavoidably accompanied

[1]Department of Chemistry, Columbia University, New York, NY, USA. [2]These authors contributed equally: Hanqing Xiong, Lixue Shi.
*e-mail: wm2256@columbia.edu

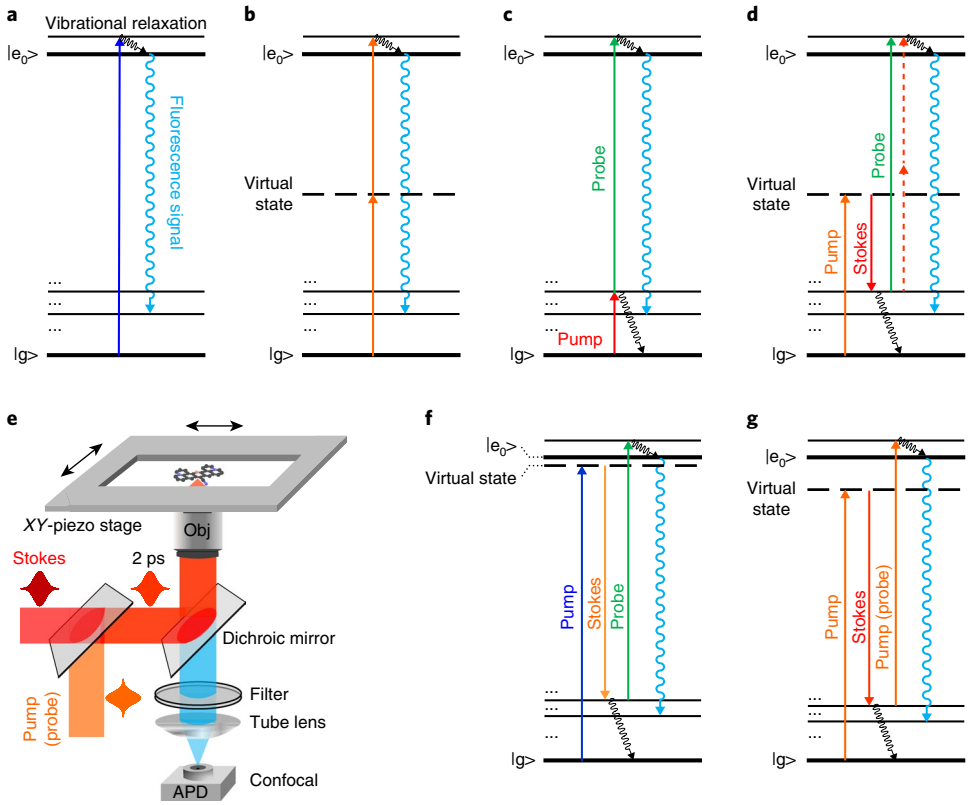


**Fig. 1 | Encoding vibrational features into fluorescence spectroscopy. a–d**, Energy diagrams of one-photon-excited fluorescence (**a**), conventional two-photon-excited fluorescence (**b**), IR-mediated double-resonance fluorescence (**c**) and SREF (**d**). **e**, Experimental set-up used in this work (details in the Methods). Temporally and spatially overlapped pump (probe) and Stokes pulse trains (2 ps, 80 MHz) are focused by a high NA objective. Backward emitted fluorescence is then detected by an APD for confocal detection. **f**, SREF with rigorous/close electronic resonance for the SRS process. **g**, SREF with appropriate electronic pre-resonance for the SRS process.

by a strong anti-Stokes fluorescence background directly excited by the pump beam, which can easily overwhelm the SREF signal.

We then realized that the linear absorption cross-section (which determines the anti-Stokes fluorescence background) can decay faster than that of (pre)resonance Raman scattering cross-section (which determines the SRS pumping rate) as a function of pump detuning of $\omega_{abs}-\omega_p$ (ref. [13]). Hence, we predicted that an appropriate pump detuning might help attenuate the anti-Stokes fluorescence background and, at the same time, largely retain the desired SREF signal. As the third attempt, we experimented on the C=C skeletal mode (Raman peak at 1,640 $cm^{-1}$) for ATTO 740 (Supplementary Fig. 2b), which corresponds to a larger pump detuning than that of the nitrile mode (Fig. 1g). Indeed, with the anti-Stokes fluorescence background decreasing by approximately a factor of 10 from the close-resonance case (Supplementary Fig. 2a, b, blue dashed curves), an obvious Raman-like peak was detected on top of the broad fluorescence excitation spectrum (Supplementary Fig. 2b, blue line in the right column). Hence, the above two tests (Supplementary Fig. 2) on the same ATTO 740 dye clearly support our strategy of retrieving the SREF peak by an appropriate electronic pre-resonance.

To demonstrate SREF as a general approach, we adopted the popular dye Rhodamine 800 (Rh800) (Fig. 2a) with a higher fluorescence quantum yield than ATTO 740 and a better collection efficiency due to its bluer emission. Rh800 bears a conjugated nitrile (C≡N) moiety with a distinct Raman peak at 2,236 $cm^{-1}$ (Fig. 2b)[14]. When $\omega_p-\omega_s$ is tuned to match the C≡N vibration, SRS is operating in the region of the electronic pre-resonance ($\omega_p$ around 838 nm, $\omega_{abs}\sim700$ nm), and the total energy $(\omega_p-\omega_s)+\omega_p$ reaches its $\omega_{abs}$ (Fig. 2a). We then obtained the SREF excitation spectrum by sweeping $\omega_p$ across the C≡N resonance with a 500 nM Rh800 solution. Remarkably, a pronounced Raman-like peak has emerged at 2,236 $cm^{-1}$ within the fluorescence excitation spectrum (Fig. 2c, solid line). Both its position and width are consistent with the corresponding SRS peak (Fig. 2b), proving its vibrational origin. As a negative control, the pump beam alone generates one-photon anti-Stokes fluorescence from the thermally excited vibrational population (Fig. 2c, blue dashed line; Supplementary Fig. 3a), and the Stokes beam alone mainly leads to two-photon-excited fluorescence (Fig. 2c, red dashed line; Supplementary Fig. 3b).

We further characterized the SREF spectroscopy. First, the time-delay dependence fits well with the cross-correlation profile of the pump and Stokes pulses (Fig. 2d). Second, the laser power dependence is linear with respect to both pump and Stokes beams (Fig. 2e,f), since the up-conversion step to the fluorescent state is already saturated with our pulsed probe (pump) laser[15] (see Methods and Supplementary Fig. 4). Third, general SREF detectability is demonstrated on further molecules in both the fingerprint region (double bond) and the cell-silent region (triple bond) (Supplementary Fig. 5). Finally, we confirmed the linear concentration dependence with a superb sensitivity readily down to 10 nM (Fig. 2g). The corresponding SREF signal is extrapolated to be 2 to 3 photons per millisecond at the single-molecule-equivalent concentration (~8 nM). Relatively poorer detection sensitivity is obtained for the C=C mode in ATTO740 (owing to its poorer fluorescence quantum yield and collection efficiency) (Supplementary Fig. 2c).

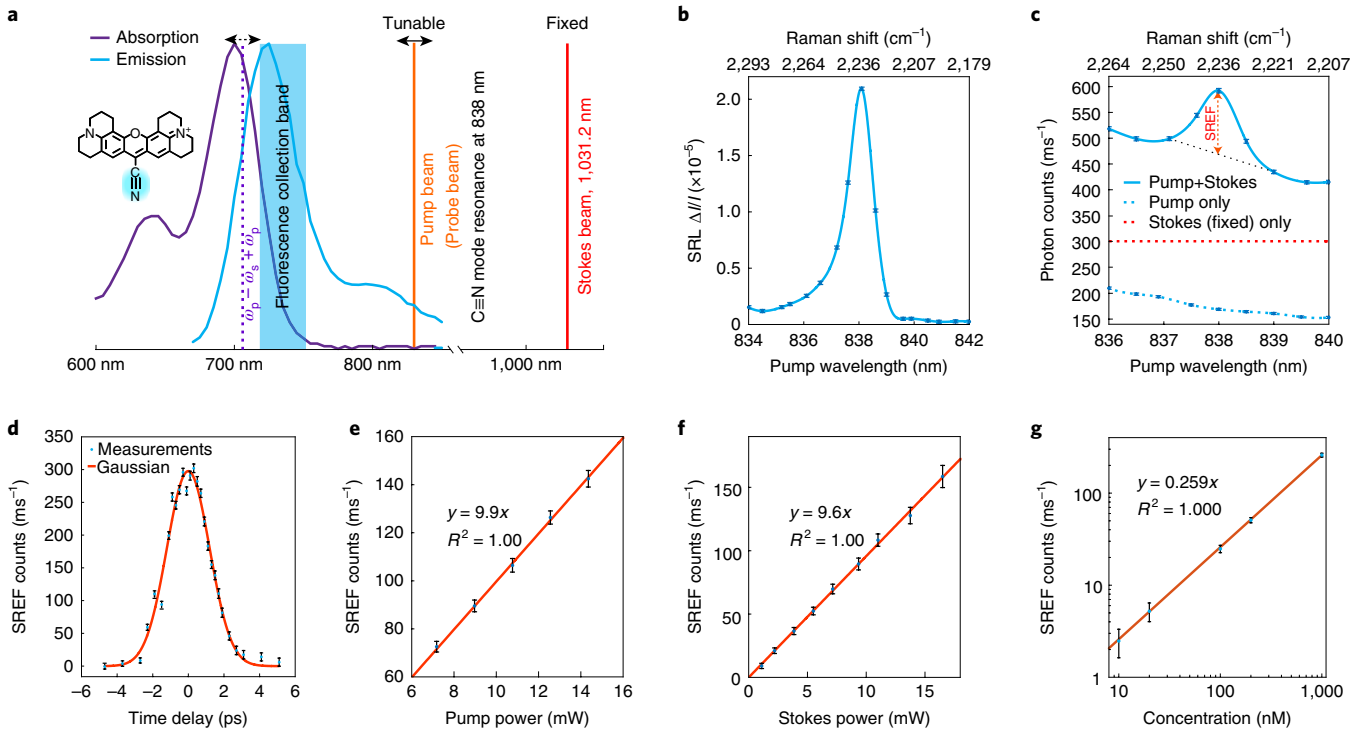


**Fig. 2 | SREF spectroscopy. a**, SREF experimental scheme on Rhodamine 800 (Rh800). Absorption (purple) and emission (blue) spectra of Rh800 in DMSO are shown, together with the tunable pump beam (orange), the fixed Stokes beam at 1,031.2 nm (red) and the energy level of $(\omega_p-\omega_s)+\omega_p$ (purple dashed line). The pump beam is also used as the probe beam. **b**, SRS spectrum for C≡N vibration of a 1 mM Rh800 solution in DMSO. **c**, SREF excitation spectrum of a 500 nM Rh800 solution in DMSO (blue solid line). The pure SREF signal size is indicated. Pump-only (blue dashed line) and Stokes-only (red dashed line) excitation results are also shown. **d**, Pure SREF signal as a function of the relative time delay between the pump and Stokes pulses. **e**, Pump-power dependence of the pure SREF signal. Stokes power set to 6 mW. **f**, Stokes-power dependence of the pure SREF signal. Pump power set to 6 mW. **g**, Dependence of pure SREF signals on the Rh800 concentration in DMSO. In **b**, **c**, **d** and **g**, $P_{pump}$ and $P_{Stokes}$ are 12 mW and 13 mW, respectively. In **b**–**g**, the error bars represent 95% confidence intervals of the mean values of normal distributions fitted by 100 independent measurements.

It is constructive to theoretically analyse the SREF signal of Rh800. A vibrational excitation rate of $8\times10^3$ per millisecond is estimated from Fig. 2b for a single C≡N bond of Rh800 under the excitation of merely a 12 mW pump beam and a 13 mW Stokes beam (see Methods). For SRS detection, the sensitivity of which is limited by laser shot noise (about $7\times10^6$ photons per millisecond for the pump beam), around 1,000 Rh800 molecules are required to overcome the shot noise. In contrast, SREF can circumvent the overwhelming laser background by upconverting some of the vibrational population to the electronic excited state for subsequent fluorescence detection. In addition to electronic pre-resonance, how to optimize the upconversion efficiency is another key. Our analysis suggests that, under our experimental conditions, the upconversion efficiency is almost totally determined by the competition between SRS pumping and the relaxation of the vibrational excited state (see Methods). We noted that vibrational relaxation often occurs very rapidly in polyatomic molecules: a vibrational lifetime of 0.5 ps is estimated by considering a predominately lifetime-broadened vibrational linewidth (~11 $cm^{-1}$ for C≡N in Rh800)[7]. That is why 2-ps-long pulses were chosen to be short enough to compete favourably with vibrational relaxation, yet long enough to maintain the fine spectral selectivity. In contrast, an inefficient pulse width of 5 ns was used in the previous unsuccessful attempt[11]. Numerically, we modelled the SREF process with a three-level rate equation, and obtained a 20% upconversion efficiency, close to the result from the steady-state approximation (see Methods and Supplementary Fig. 4). This corresponds to a SREF excitation rate of about $1.6\times10^3$ per millisecond. Considering the 16% fluorescence quantum yield[16] and an overall 2% microscope fluorescence collection, a moderate signal of 5 photons per millisecond is theoretically estimated from a single Rh800 molecule, which agrees well with experimental measurement (extrapolated to ~8 nM in Fig. 2g).

SREF combines the desirable properties of chemical specificity and superb sensitivity, thereby going beyond the standard fluorescence and Raman spectroscopy. To showcase the exquisite vibrational selectivity of SREF, we synthesized a set of new isotopologues for the Rh800-containing isotopically edited nitrile moiety (Fig. 3a, $^{12}C\equiv^{15}N$, $^{13}C\equiv^{14}N$ and $^{13}C\equiv^{15}N$; synthesis in Supplementary Information). As expected, the absorption and emission spectra are identical among these isotopologues, preventing their spectral separation by standard fluorescence techniques (Fig. 3b). In contrast, spectrally well-resolved SREF peaks from C≡N vibrations can be successfully acquired for four isotopologues (Fig. 3c and Supplementary Fig. 6), in agreement with the corresponding Raman peak positions[14] (Fig. 3c, dashed lines).

By leveraging the fine vibrational specificity, we then demonstrate multiplexed SREF imaging. There is increasing demand for simultaneously imaging a large number of molecular targets in complex systems[17]. However, due to the limited chemical specificity, fluorescence microscopy exhibits a fundamental 'colour barrier': in practice, no more than five fluorescent dyes can be simultaneously imaged[18]. In our multiplexed SREF imaging, a single SREF image is obtained by sample raster scanning for a given $\omega_p$ (see Methods); a stack of hyperspectral images is then acquired by sweeping $\omega_p$. As a proof of concept, living *Escherichia coli* (*E.coli*) cells (Fig. 3d), each stained with one of the four Rh800 isotopologues and then mixed

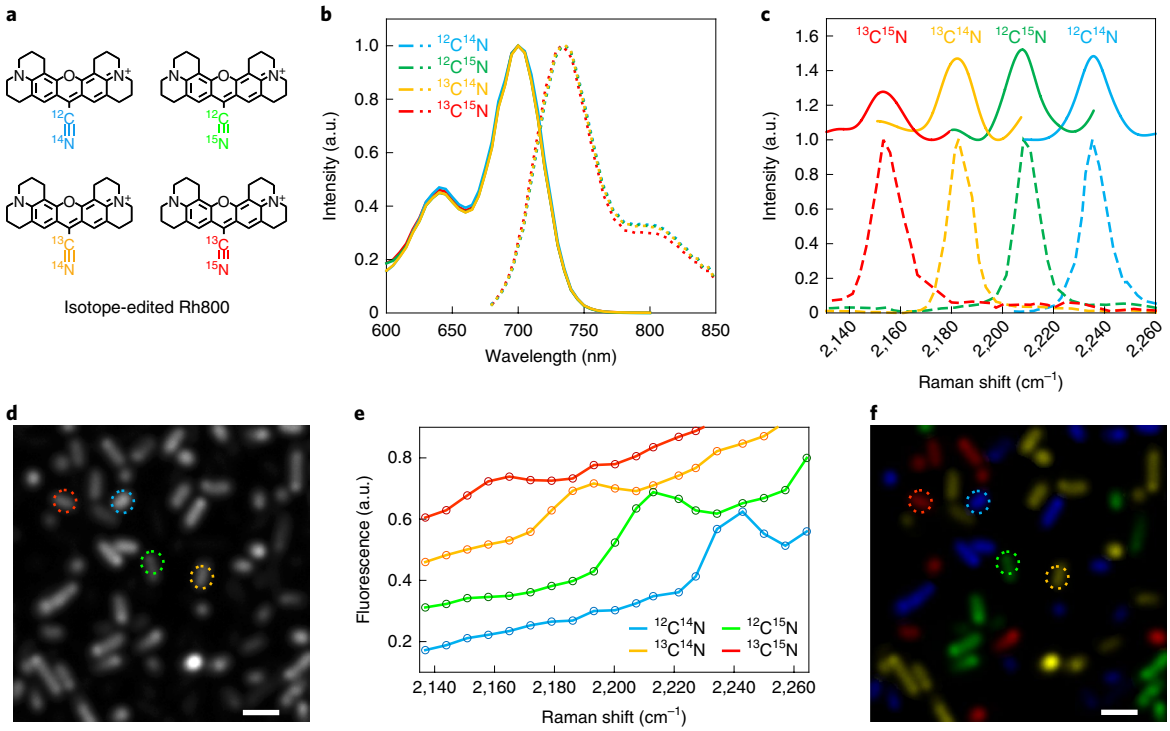


**Fig. 3 | Living-cell multicolour SREF microscopy. a**, Chemical structures of Rh800 and its three derivatives with isotopically edited nitrile bonds. **b**, Absorption and emission spectra for four Rh800 isotopologues. **c**, SREF excitation spectra (colour-coded solid lines) and the corresponding SRS spectra (colour-coded dashed lines) for four Rh800 isotopologues in DMSO. **d**,**f**, Fluorescence imaging (**d**) and multicolour SREF imaging (**f**) of living *E. coli* stained by four Rh800 isotopologues. **e**, SREF spectra of cells marked by the corresponding circles in **d** and **f**. In **f**, colours are coded with respect to the corresponding SREF spectra. Scale bars, 2 μm. a.u., arbitrary units.

together, could be unequivocally resolved by the detected SREF peak (Fig. 3e) and assigned back to the corresponding Rh800 isotopologues (Fig. 3f). Thus, when coupled with newly developed palettes of vibrational probes[17], multiplexed SREF imaging can break the 'colour barrier' of fluorescence and holds the promise for super-multiplex optical microscopy.

We now demonstrate all-far-field vibrational imaging of single molecules at room temperature. We note that previous single-molecule Raman spectroscopy is possible in the optical near-field only with the help of strong plasmonic enhancement[5,19–22]. Electronic resonance on light-absorbing chromophores is also indispensable for nearly all single-molecule surface-enhanced Raman spectroscopy: detecting single-molecule non-resonant molecules is extremely rare. Nonetheless, the strict reliance on close contact to metallic nanostructures (ångstrom-level precision) has limited the applicability of these near-field techniques in vast chemical and biological systems[23]. In retrospect, single-molecule fluorescence spectroscopy made its major impact in chemistry and biology after it transitioned from near-field to far-field. In light of this, single-molecule far-field Raman spectroscopy would have the potential to impact many areas where metallic nanostructures are inaccessible or undesirable.

For imaging single molecules in the far field, we followed standard sample preparations for embedding Rh800 in PMMA film[24] and validated the spectroscopic preservation using absorption, fluorescence and SREF spectra of Rh800 isotopologues (Fig. 4a,b and Supplementary Fig. 7). To assist locating and confirming individual molecules, a 660-nm continuous-wave laser was used for one-photon fluorescence (details in Methods and Supplementary Fig. 1). Single-molecule distribution could be evidenced by abrupt photobleaching during raster scanning (half-moon pattern in Fig. 4c), occasional blinking, and single-step beaching time traces (Supplementary Fig. 8). We next acquired single-molecule SREF spectral images by sweeping $\omega_p$ across the vibrational resonance of C≡N in Rh800. Consistently, a more pronounced signal is observed at the on-resonance frequency for multiple molecules within the same field-of-view (Fig. 4d,e), as well as in repetitive pump scans over the same molecule (Fig. 4f,g). The peak position, shape and linewidth all resemble the bulk SREF measurement, confirming the vibrational resonance (Fig. 4d–i). Quantitatively, about 4 photons per millisecond were detected from the brightest pixel from on-resonance images (Supplementary Fig. 9), comparable to the solution measurement. The single-molecule identity and its survival are further confirmed by additional 660-nm-excited fluorescence following the SREF series and subsequent single-step photobleaching.

Such ultimate sensitivity is extendable to Rh800 isotopologues that are vibrationally distinct but electronically identical (Fig. 4h,i). By sweeping $\omega_p$ across the corresponding vibrational resonance, sharp SREF image contrasts were clearly observed at the expected Raman shifts for both $^{12}C{\equiv}^{15}N$ (2,207 $cm^{-1}$) and $^{13}C{\equiv}^{14}N$ (2,183 $cm^{-1}$) (Fig. 4h,i). Such fine chemical specificity at the single-molecule level would be extremely difficult, if not impossible, to achieve by room-temperature fluorescence spectroscopy or absorption spectroscopy[2,25–28]. We further confirmed Raman selectivity of single-molecule SREF spectral images by conducting statistical tests over 61 complete image sets. For each set, we performed a Student's *t*-test between on-resonance signals and two adjacent off-resonance signals, respectively, as well as between the two off-resonance channels (Fig. 4j, Supplementary Table 1). In most sets (53 out of 61), the on-resonance signals are statistically higher than the off-resonance backgrounds ($P < 0.05$). In contrast, no significant difference can be found between the two off-resonance channels. Interestingly, the signal-to-background ratios (on/off ratio) (Fig. 4k) show a broad

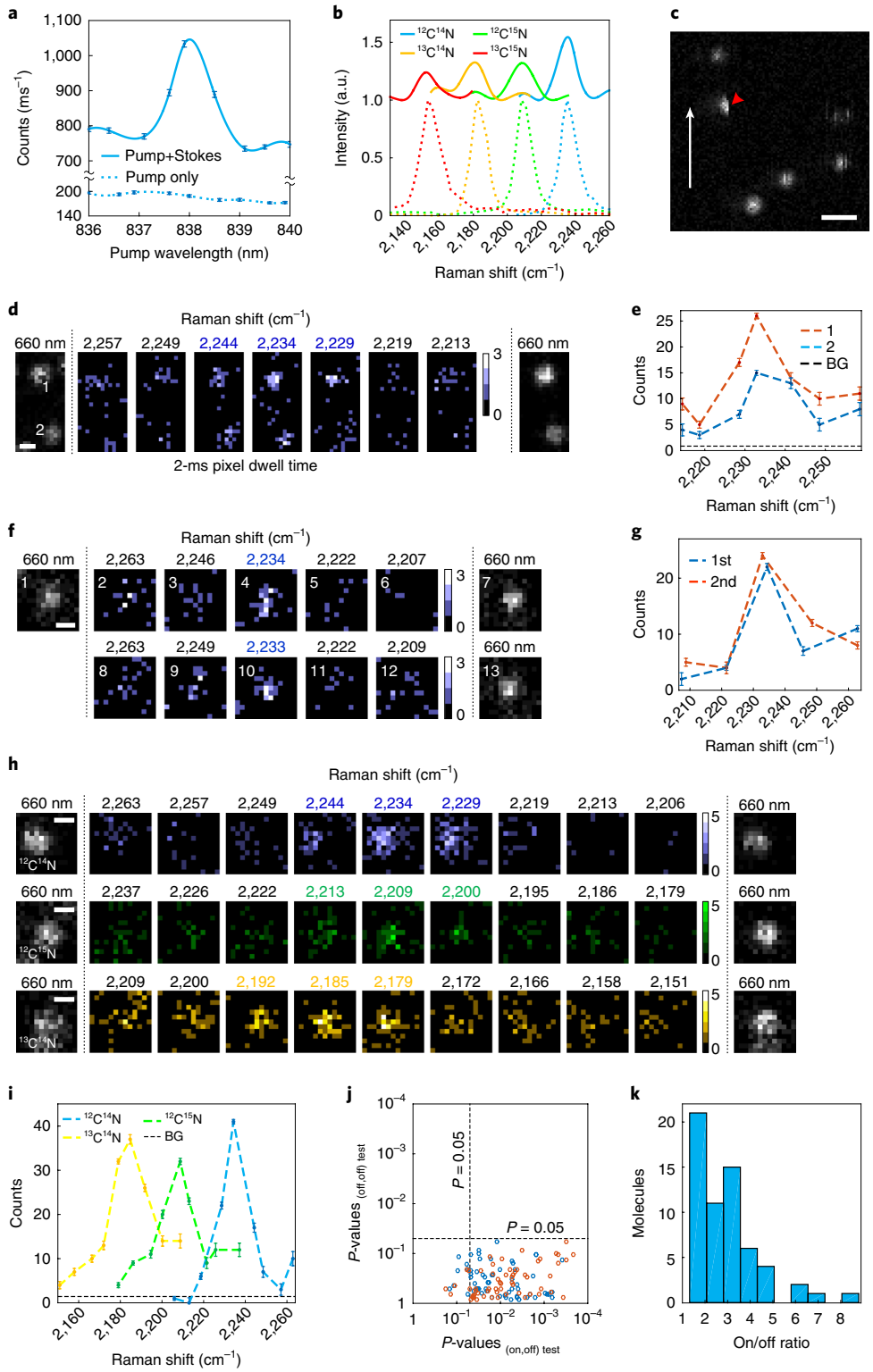


**Fig. 4 | Single-molecule SREF spectroscopy and imaging. a**,**b**, Ensemble SREF excitation spectra of Rh800 (**a**) and its isotopologues (**b**) in PMMA films. Colour-coded dashed lines in **b** show the corresponding SRS spectra. **c**, Single-molecule fluorescence image excited by a 660-nm continuous-wave laser. The white arrow shows the fast axis of the raster scanning. The red arrowhead indicates 'half-moon' photobleaching. Scale bar, 1 μm. **d**,**e**, Recording single-molecule SREF spectra of two Rh800 molecules simultaneously (red dashed line, molecule 1; blue dashed line, molecule 2). BG, background. **f**,**g**, Recording SREF spectra of the same molecule by two rounds (blue dashed, first round; red dashed, second round). **h**,**i**, Single-molecule SREF images of Rh800 isotopologues. In **d**, **f** and **h**, the imaging sequence was initial fluorescence imaging (660-nm laser-excited), sequential SREF spectral imaging and final fluorescence imaging (660-nm laser-excited). Colour bars, counts per 2 ms. Scale bars, 400 nm. In **e**, **g** and **i**, photon counts are the sum of photons within the 5 × 5-pixel centre areas of the corresponding images, and the error bars are the average and standard deviation of photon counts of nearby 50 molecule-free 5 × 5-pixel regions. **j**, Student's *t*-test of signals between the on-resonance channel and its adjacent two off-resonance channels (blue and red circles, respectively), and between the two off-resonance channels for 61 sets of single-molecule SREF images. **k**, On/off ratio distribution of the 61 sets.

distribution, which probably originated from random orientations of individual Rh800 within PMMA film and the possible mismatch of dipole moments between SREF and two-photon fluorescence (Supplementary Fig. 10). To the best of our knowledge, this is the first all-far-field Raman spectroscopy of single molecules[29,30].

In this work, we have integrated both the desired chemical selectivity and the superb sensitivity into a new Raman-mediated multiphoton fluorescence process of SREF. Different from a previous attempt[11], an electronic pre-resonance is devised and the upconversion efficiency is optimized to ensure successful SREF detection above competing backgrounds. Agreement was found between theory (see Methods) and experiments for Rh800 and its isotopologues. Clear SREF spectroscopy of different Raman modes was recorded in several other dyes in both the fingerprint region and the cell-silent region (Fig. 3c, Supplementary Fig. 2, 5), supporting its general applicability. Most notably, single-molecule Raman spectroscopy and imaging are achieved in the optical far-field (Fig. 4), bypassing the need for plasmonic enhancement. This would have profound implications, in light of the revolutionary impact of far-field single-molecule fluorescence spectroscopy. Besides spectroscopic applications, SREF also has great potential for biological imaging. Owing to its superior detection sensitivity over SRS (by about 100 times), multiplexed SREF would provide a more sensitive technique for super-multiplex vibrational imaging[17]. With the single-molecule imaging capability, localization-based methods would enable super-resolution vibrational imaging.

Further technical improvements would promise even higher signals and richer spectral information. For example, using fluorophores with higher quantum yields (only 16% for Rh800 and 10% for ATTO740) could result in much brighter SREF signals; a more sophisticated laser source with both tunable pump and Stokes beams, and ideally a separate probe beam, could allow more flexible excitation control, enabling SREF investigation of many more molecules across the wide spectrum.

## Online content

Any methods, additional references, Nature Research reporting summaries, source data, statements of data availability and associated accession codes are available at https://doi.org/10.1038/s41566-019-0396-4.

Received: 18 January 2019; Accepted: 20 February 2019;
Published online: 1 April 2019

## References

1. Lakowicz, J. R. *Principles of Fluorescence Spectroscopy* 3rd edn (Springer US, New York, 2007).
2. Moerner, W. & Orrit, M. Illuminating single molecules in condensed matter. *Science* **283**, 1670–1676 (1999).
3. Schatz, G. C. & Ratner, M. A. *Quantum Mechanics in Chemistry* (Courier Corp., New York, 1993).
4. Herzberg, G. *Infrared and Raman Spectra of Polyatomic Molecules* Vol. 2 (D. Van Nostrand, New York, 1945).
5. Nie, S. & Emory, S. R. Probing single molecules and single nanoparticles by surface-enhanced Raman scattering. *Science* **275**, 1102–1106 (1997).
6. Seilmeier, A., Kaiser, W., Laubereau, A. & Fischer, S. A novel spectroscopy using ultrafast two-pulse excitation of large polyatomic molecules. *Chem. Phys. Lett.* **58**, 225–229 (1978).
7. Hübner, H.-J., Wörner, M., Kaiser, W. & Seilmeier, A. Subpicosecond vibrational relaxation of skeletal modes in polyatomic molecules. *Chem. Phys. Lett.* **182**, 315–320 (1991).
8. Mastron, J. N. & Tokmakoff, A. Two-photon-excited fluorescence-encoded infrared spectroscopy. *J. Phys. Chem. A* **120**, 9178–9187 (2016).
9. Cheng, J. & Xie, X. Coherent anti-Stokes Raman scattering microscopy: instrumentation, theory, and applications. *J. Phys. Chem. B* **108**, 827–840 (2004).
10. Min, W., Freudiger, C. W., Lu, S. & Xie, X. S. Coherent nonlinear optical imaging: beyond fluorescence microscopy. *Annu. Rev. Phys. Chem.* **62**, 507–530 (2011).
11. Lee, S., Nguyen, D. & Wright, J. Double resonance excitation of fluorescence by stimulated Raman scattering. *Appl. Spectrosc.* **37**, 472–474 (1983).
12. Shim, S., Stuart, C. M. & Mathies, R. A. Resonance Raman cross-sections and vibronic analysis of Rhodamine 6G from broadband stimulated Raman spectroscopy. *ChemPhysChem* **9**, 697–699 (2008).
13. Wei, L. & Min, W. Electronic preresonance stimulated Raman scattering microscopy. *J. Phys. Chem. Lett.* **9**, 4294–4301 (2018).
14. Etchegoin, P. G., Le, Ru,E. C. & Meyer, M. Evidence of natural isotopic distribution from single-molecule SERS. *J. Am. Chem. Soc.* **131**, 2713–2716 (2009).
15. Min, W. et al. Imaging chromophores with undetectable fluorescence by stimulated emission microscopy. *Nature* **461**, 1105–1109 (2009).
16. Sperber, P., Spangler, W., Meier, B. & Penzkofer, A. Experimental and theoretical investigation of tunable picosecond pulse generation in longitudinally pumped dye laser generators and amplifiers. *Opt. Quant. Electron.* **20**, 395–431 (1988).
17. Wei, L. et al. Super-multiplex vibrational imaging. *Nature* **544**, 465–470 (2017).
18. Dean, K. M. & Palmer, A. E. Advances in fluorescence labeling strategies for dynamic cellular imaging. *Nat. Chem. Biol.* **10**, 512–523 (2014).
19. Kneipp, K. et al. Single molecule detection using surface-enhanced Raman scattering (SERS). *Phys. Rev. Lett.* **78**, 1667–1670 (1997).
20. Sonntag, M. D. et al. Single-molecule tip-enhanced Raman spectroscopy. *J. Phys. Chem. C* **116**, 478–483 (2011).
21. Yampolsky, S. et al. Seeing a single molecule vibrate through time-resolved coherent anti-Stokes Raman scattering. *Nat. Photon.* **8**, 650–656 (2014).
22. Zhang, Y. et al. Coherent anti-Stokes Raman scattering with single-molecule sensitivity using a plasmonic Fano resonance. *Nat. Commun.* **5**, 4424 (2014).
23. Mahmoudi, M. et al. Protein–nanoparticle interactions: opportunities and challenges. *Chem. Rev.* **111**, 5610–5637 (2011).
24. Macklin, J., Trautman, J., Harris, T. & Brus, L. Imaging and time-resolved spectroscopy of single molecules at an interface. *Science* **272**, 255–258 (1996).
25. Nie, S., Chiu, D. T. & Zare, R. N. Probing individual molecules with confocal fluorescence microscopy. *Science* **266**, 1018–1021 (1994).
26. Kukura, P., Celebrano, M., Renn, A. & Sandoghdar, V. Single-molecule sensitivity in optical absorption at room temperature. *J. Phys. Chem. Lett.* **1**, 3323–3327 (2010).
27. Chong, S., Min, W. & Xie, X. S. Ground-state depletion microscopy: detection sensitivity of single-molecule optical absorption at room temperature. *J. Phys. Chem. Lett.* **1**, 3316–3322 (2010).
28. Gaiduk, A., Yorulmaz, M., Ruijgrok, P. & Orrit, M. Room-temperature detection of a single molecule's absorption by photothermal contrast. *Science* **330**, 353–356 (2010).
29. Zrimsek, A. et al. Single-molecule chemistry with surface- and tip-enhanced Raman spectroscopy. *Chem. Rev.* **117**, 7583–7613 (2017).
30. Winterhalder, M., Zumbusch, A., Lippitz, M. & Orrit, M. Toward far-field vibrational spectroscopy of single molecules at room temperature. *J. Phys. Chem. B* **115**, 5425–5430 (2011).

## Acknowledgements

We are grateful for discussions with L. E. Brus and X. Y. Zhu. This work was supported by grant R01GM128214 from the NIH, and by the Camille and Henry Dreyfus Foundation.

## Author contributions

H.X. and L.S. collected and analysed all the data; H.X. designed and constructed the instrument with the help of L.S. and Z.Z. under the guidance of W.M.; L.W. and Y.S. contributed to the early phase of the spectroscopy project; R.L. performed chemical synthesis; W.M. conceived the concept; H.X., L.S. and W.M. wrote the manuscript with input from all authors.

## Additional information

**Supplementary information** is available for this paper at https://doi.org/10.1038/s41566-019-0396-4.

**Reprints and permissions information** is available at www.nature.com/reprints.

**Correspondence and requests for materials** should be addressed to W.M.

**Publisher's note:** Springer Nature remains neutral with regard to jurisdictional claims in published maps and institutional affiliations.

## Methods

**System configuration of lasers and microscope.** A comprehensive experimental scheme is shown in Supplementary Fig. 1. A picoEmerald S (Applied Physics & Electronics, Inc.) system was used to provide synchronized Stokes and pump beams for SRS and SREF measurements. The fundamental 1,031.2 nm IR fibre laser (2 ps pulse width and 80 MHz repetition rate, 0.5 nm full-width at half-maximum (FWHM) bandwidth) is adopted as our Stokes beam. A part of the IR laser was frequency-doubled to synchronously seed the optical parametric oscillator system and produce a tunable pump beam (2 ps pulse width, 0.5 nm FWHM bandwidth). The idler beam was blocked. All beams are linearly polarized in the same direction. Pump and Stokes beams were expanded and coupled into an Olympus IX71 microscope to overfill the back pupil of the objective for diffraction-limited imaging. A 60× water immersion objective (UPLSAPO, 1.2 NA, Olympus) was used for all measurements. Two raster scanning methods were used for imaging: stage scanning for single-molecule imaging and laser scanning for living-cell imaging. Stage-scan was achieved with a XY piezo stage (P545, Physik Instrumente); laser scanning was achieved with a standard 2D-galvanometer (GVSM002, Thorlabs). All imaging scanning and data acquisition were controlled by in-house-written LabVIEW programs.

For SRS (stimulated Raman loss, SRL) detection, the Stokes beam was modulated at 20 MHz by an electro-optical modulator (EOM) to achieve shot-noise-limited detection. The forward-going pump and Stokes beams after the samples were collected by a high NA IR-coated oil condenser (1.4 NA, Olympus), which is aligned by Köhler illumination. A high-speed, large-area silicon PIN photodiode (S3590-09, Hamamatsu) was used as the detector. A high optical density bandpass filter (ET890/220 m, Chroma) was placed in front of the photodiode to block the Stokes beam completely and transmit the pump beam. The photodiode was reverse biased by 64 V from a DC power supply to increase both the saturation threshold and response bandwidth. The signal output of the photodiode was then sent to a fast lock-in amplifier (HF2LI, Zurich Instruments) for signal demodulation. The demodulated signal was digitalized by a NI card (PCI-6259, NI) driven by our in-house-written LabVIEW program.

In SREF, the Stokes laser is not modulated. For SREF detection of Rh800 and MARS dyes (both nitrile bond and C=C bond), pump and Stokes beams pass through a dichroic mirror (FF825-SDi01, Semrock) to excite the molecules, and the backward fluorescence is then detected. Two bandpass filters (FF01-709/167-25, Semrock), each with an optical density greater than 6, are used to block the reflected laser beams, and another bandpass filter (FF01-735/28-25, Semrock) with an optical density greater than 7 is adopted to completely block the CARS background. For SREF detection of the ATTO740 C=C bond, the corresponding dichroic mirror is FF825-SDi01 (Semrock) and the filters include two bandpass filters (FF01-819/44-25, Semrock). For SREF detection of the ATTO740 nitrile bond, the corresponding dichroic mirror is FF825-SDi01 (Semrock) and the filters include two bandpass filters (FF01-709/167-25, Semrock) for blocking the reflected laser beams, and another bandpass filter (FF01-785/62-25, Semrock) for completely blocking the CARS background. A high-quantum-yield (~70% at 700-nm) single-photon counting module (SPCM) (SPCM-NIR-14-FC, 70-cps dark counts, Excelitas) was used to detect fluorescent emission for general measurements, and a similar quantum-yield SPCM but with much lower dark counts (SPCM-AQRH-16-FC, 7 cps dark counts, Excelitas) was used for the single-molecule SREF imaging presented in Fig. 4. The 100 µm active APD diameter forms a loose confocal configuration for detection and imaging.

For parallel single-molecule fluorescence detection, an additional 660-nm continuous-wave laser (Coherent) was coupled into the microscope. A quarter-wave plate was used to transform the linear polarization to circular polarization. For 660-nm continuous-wave laser-excited fluorescence detection of Rh800, the laser is passed through a dichroic mirror (690dcxr, Chroma) and fluorescence is collected after two bandpass filters (FF01-795/150-25, Semrock; FF01-747/33-25, Semrock).

**Physical model for SREF signal estimation.** Since the electronic coherence dies out in the condensed phase at room temperature within tens of femtoseconds[31], and our SRS excitation rate is much slower than the decay rate of vibrational coherence[32], it is feasible to model the SREF process by the rate equations of a three-level system[33,34]. The energy-level diagram is shown in Supplementary Fig. 4a. $N_1$, $N_2$ and $N_3$ represent the population on the corresponded states. $W_{12}$ is the epr-SRS excitation rate, $w_{21}$ is the vibrational relaxation rate for targeted vibrational mode, $W_{23}$ is the probe excitation rate from the vibrational excited state to the electronic excited state. All other transition processes are omitted because of much lower transition rates. The rate equation of the system can thus be written as:

$$\frac{dN_1}{dt} = W_{12}(N_2 - N_1) + w_{21}N_2 \quad (1)$$

$$\frac{dN_2}{dt} = W_{23}(N_3 - N_2) + W_{12}(N_1 - N_2) - w_{21}N_2 \quad (2)$$

$$\frac{dN_3}{dt} = W_{23}(N_2 - N_3) \quad (3)$$

We first consider the epr-SRS process for the C≡N Raman mode in Rh800. The epr-SRS excitation probability at the C≡N resonance is measured to be $\Delta I/I = 2\times10^{-5}$ per pump pulse with a 1 mM Rh800 DMSO solution, under a 12 mW pump beam (838 nm) and a 13 mW Stokes beam (1,031.2 nm). With an 80 MHz repetition rate, one 2-ps-long pump pulse contains $6\times10^8$ photons at this power, which indicates $1.2\times10^4$ SRS transitions in one pulse duration. There are about $1.2\times10^5$ molecules in the focal volume with an NA 1.2 objective and a 1 mM concentration ($2.0\times10^{-13}$ cm$^3$ focal volume[35]). Hence, the epr-SRS transition probability is about 0.1 per molecule per pulse under these conditions. Moreover, the transition rate for $W_{12}$ is $1.2\times10^4/(1.2\times10^5\times2\times10^{-12}\,\text{s}) = 5\times10^{10}$ per molecule per second (s) within the pulse duration. This represents an average epr-SRS transition rate of $5\times10^{10}\,\text{s}\times2\times10^{-12}\,\text{s}\times80\,\text{MHz} = 8\times10^3$ per molecule per millisecond. The linewidth of the C≡N mode of Rh800 was measured to be 11 cm$^{-1}$, indicating a 0.5 ps lifetime ($\tau_{21}$)[7]. Therefore, we have $w_{21} = 2\times10^{12}\,\text{s}^{-1}$. The absorption cross-section for Rh800 at the peak absorption wavelength is $4\times10^{-16}$ cm$^2$. Assuming a Franck–Condon factor of 0.1, a value reasonable for many electronically coupled vibrational modes[7], $W_{23}$ is then $6\times10^8\times0.1\times4\times10^{-16}\,\text{cm}^2/(1.2\times10^{-9}\,\text{cm}^2\times2\times10^{-12}\,\text{s}) = 10^{13}\,\text{s}^{-1}$ (the focal area is $1.2\times10^{-9}$ cm$^2$) per pulse duration (it should be noted that if even the Franck–Condon factor is ten times smaller, the solution of equations (1)–(3) showed no obvious change). Obviously, because both probe process (time constant determined by $W_{23}$) and the SRS pumping process (time constant determined by $w_{21}$) have a time constant smaller than the laser pulse width, the steady-state solution of equations (1)–(3) should be a good approximation

$$N_3 = N_2 = N_1\frac{W_{12}}{w_{21}+W_{12}} \approx N_1\frac{W_{12}}{w_{21}} = \tau_{12}W_{12}N_1 \approx \tau_{12}W_{12}N \quad (4)$$

Note that $W_{12}$ is much smaller than $w_{21}$ here, hence, $N_1 \approx N$, the total molecule number in the laser focus. So, SREF emission rate, $W_{SREF}$, can be represented as

$$W_{SREF} = f_{rep}N_3\eta = f_{rep}\tau_{12}W_{12}N\eta \propto f_{rep}\tau_{12}\sigma I_p I_s N\eta \quad (5)$$

where $f_{rep}$ is the laser repetition rate; $I_p$ and $I_s$ are the intensities of the pump and Stokes laser beams, respectively; $\sigma$ is the (pre-resonance) spontaneous Raman cross-section of the C≡N Raman mode; $\eta$ is the fluorescence quantum yield of Rh800. Equation (5) shows that the SREF signal is proportional to the molecule concentration, Stokes beam intensity, pump beam intensity, vibrational state lifetime and laser repetition rate, as long as the time interval between two adjacent pulses is longer than the fluorescence lifetime.

With the obtained parameters of $W_{12}$, $w_{21}$, $W_{23}$, we also numerically calculated the population dynamics of a 50 µM Rh800 DMSO solution (6,000 molecules in the focal volume) in one pulse duration of 2 ps. The readers can check that the result is very close to the steady state result equation (4). The initial populations at the beginning of the pulse are set to $N_1 = 6{,}000$, $N_2 = N_3 = 0$. Numerically solving the equations (1)–(3) within a pulse duration of 2 ps, the time-evolved solutions in Supplementary Fig. 4b show that both $N_2$ and $N_3$ reach about 120 at the end of the pulse. This result indicates that the probability for one molecule being excited to the electronic transition state after one pulse excitation is 2% (=120/6,000), corresponding to a single-molecule SREF transition rate of 80,000 pulses per millisecond × 0.02 per pulse = 1,600 per millisecond. The coupling efficiency between epr-SRS and the probe process is hence $1{,}600/8\times10^3 = 20\%$. With a 16% fluorescence quantum yield[16] of Rh800 dye molecule and a collection efficiency ~2% of our microscope (estimated including all optics and electronic yield), the SREF signal size for one molecule equals $80{,}000\times0.02\times0.16\times0.02 \approx 5$ photons per millisecond.

It is worth noting that, due to the sub-picosecond lifetime of vibrational relaxation, only a small fraction of the SRS transitions can be successfully transferred as a population at the electronic excited state, which contributes to the SREF signal. Under the steady-state approximation, the coupling efficiency of the probing process can be simply represented as

$$\eta_c = \frac{N_3}{N_1W_{12}\tau_{pulse}} = \frac{\tau_{12}W_{12}N_1}{N_1W_{12}\tau_{pulse}} = \frac{\tau_{12}}{\tau_{pulse}} \quad (6)$$

Here $\tau_{pulse}$ is the pulse width. For our system, equation (6) gives 0.5 ps/2 ps = 25%, which is very close to the numerical simulation shown above. To increase the coupling efficiency without losing the spectral resolution, the shortest pulse for SREF excitation is around 1 ps for a Fourier transform-limited pulse laser system (bandwidth ~10 cm$^{-1}$).

**Experimental procedures for SREF spectroscopy and imaging.** *Materials for sample preparation.* Dimethyl sulfoxide (DMSO) (Sigma, D8418), toluene (Sigma, 650579), Rhodamine 800 (Rh800) (Sigma, 83701), ATTO740 (ATTO-TEC, AD 740-21), PMMA (Electron Microscopy Sciences, PMMA powder in the kit, 14655), sulfate acid (Sigma, 258105), hydrogen peroxide solution (30 wt% in water) (Sigma, 216763).

*Staining and imaging of living E. coli* cells. For the analysis shown in Fig. 3, cells were incubated with 0.5 μM Rh800 in PBS for 15 min at room temperature for different isotopologues, then centrifuged and washed with PBS at room temperature before mixing together. After mixing, the cells were seeded on polylysine-coated coverslip for SREF imaging. The pixel dwell time of the galvanometer-driven raster scanning system was set to 10 μs. Nineteen-frame SREF image series were acquired by fixing the Stokes beam at 1,031.2 nm and scanning the pump beam through the 836.5–845.5 nm range with a 0.5 nm step size. $P_{pump}$ and $P_{Stokes}$ were 12 mW and 10 mW, respectively.

*Single-molecule sample preparation.* PMMA solution (1 wt% in toluene) was prepared by directly dissolving PMMA powder in toluene. A 10 mM Rh800 DMSO solution was pre-diluted to 1 nM in toluene, and further diluted to 50 pM in above PMMA solution. Finally, the 50 pM Rh800 PMMA solution was spin-coated (5,000 r.p.m., Laurell Technologies Corporation) onto a quartz coverslip (Alfa Aesar) to form PMMA-embedded single-molecule specimen. Quartz coverslips were cleaned by first soaking in Piranha solution ($H_2SO_4$: $H_2O_2$ solution = 3:1 v/v) at 90 °C overnight, followed by 30 min ultrasonic cleaning in deionized water repeated more than four times.

*SREF spectroscopy and imaging of Rh800 and its isotopologues.* For the ensemble SREF spectra recording of Rh800 and its isotopologues in PMMA films shown in Fig. 4, samples were prepared by spin-coating 500 nM corresponding dyes in 1% PMMA toluene onto quartz coverslips. $P_{pump}$ and $P_{Stokes}$ were 12 mW and 13 mW, respectively. For single-molecule SREF imaging shown in Fig. 4, the imaging sequence was initial fluorescence imaging (660-nm laser-excited), sequential SREF spectral imaging series and final fluorescence imaging again. Pixel sizes were set to 100 nm × 100 nm and the pixel dwell time was set to 2 milliseconds. $P_{pump}$ and $P_{Stokes}$ were 8 mW and 6 mW, respectively.

*Single-molecule statistical analysis.* For the Student's *t*-test of 61 sets of single-molecule SREF images shown in Fig. 4, signals of 25 pixels in the 5 × 5-pixel centre areas of corresponding images were used. *P* values of on/off tests are the results of one-tailed paired *t*-tests between the on-resonance channel (pump wavelength = 838 nm) and the two adjacent off-resonance channels (pump wavelength = 837 nm and 839 nm), respectively; the *P* values of off/off control tests are the results of a two-tailed paired *t*-test between the high-energy-side off-resonance channel (pump wavelength = 837 nm) and the low-energy-side off-resonance channel (pump wavelength = 839 nm). On/off ratios were calculated by dividing the on-channel signal by the average signal of the two adjacent off-resonance channels.

## Data availability

The data that support the plots within this paper and other findings of this study are available from the corresponding author upon reasonable request.

## References

31. Brinks, D. et al. Ultrafast dynamics of single molecules. *Chem. Soc. Rev.* **43**, 2476–2491 (2014).
32. Kukura, P., McCamant, D. W. & Mathies, R. A. Femtosecond stimulated Raman spectroscopy. *Annu. Rev. Phys. Chem.* **58**, 461–488 (2007).
33. Siegman, A. E. *Lasers.* (University Science Books, Mill Valley, CA, 1986).
34. Wright, J. C. Double resonance excitation of fluorescence in the condensed phase—an alternative to Infrared, Raman, and fluorescence spectroscopy. *Appl. Spectrosc.* **34**, 151–157 (1980).
35. Zipfel, W. R., Williams, R. M. & Webb, W. W. Nonlinear magic: multiphoton microscopy in the biosciences. *Nat. Biotechnol.* **21**, 1369–1377 (2003).

Nature Research, brought to you courtesy of Springer Nature Limited (“Nature Research”)

Terms and Conditions

Nature Research supports a reasonable amount of sharing of content by authors, subscribers and authorised or authenticated users (“Users”), for small-scale personal, non-commercial use provided that you respect and maintain all copyright, trade and service marks and other proprietary notices. By accessing, viewing or using the nature content you agree to these terms of use (“Terms”). For these purposes, Nature Research considers academic use (by researchers and students) to be non-commercial.

These Terms are supplementary and will apply in addition to any applicable website terms and conditions, a relevant site licence or a personal subscription. These Terms will prevail over any conflict or ambiguity with regards to the terms, a site licence or a personal subscription (to the extent of the conflict or ambiguity only). By sharing, or receiving the content from a shared source, Users agree to be bound by these Terms.

We collect and use personal data to provide access to the nature content. ResearchGate may also use these personal data internally within ResearchGate and share it with Nature Research, in an anonymised way, for purposes of tracking, analysis and reporting. Nature Research will not otherwise disclose your personal data unless we have your permission as detailed in the Privacy Policy.

Users and the recipients of the nature content may not:

1. use the nature content for the purpose of providing other users with access to content on a regular or large scale basis or as a means to circumvent access control;
2. use the nature content where to do so would be considered a criminal or statutory offence in any jurisdiction, or gives rise to civil liability, or is otherwise unlawful;
3. falsely or misleadingly imply or suggest endorsement, approval , sponsorship, or association unless explicitly agreed to by either Nature Research or ResearchGate in writing;
4. use bots or other automated methods to access the nature content or redirect messages; or
5. override any security feature or exclusionary protocol.

These terms of use are reviewed regularly and may be amended at any time. We are not obligated to publish any information or content and may remove it or features or functionality at our sole discretion, at any time with or without notice. We may revoke this licence to you at any time and remove access to any copies of the shared content which have been saved.

Sharing of the nature content may not be done in order to create substitute for our own products or services or a systematic database of our content. Furthermore, we do not allow the creation of a product or service that creates revenue, royalties, rent or income from our content or its inclusion as part of a paid for service or for other commercial gain. Nature content cannot be used for inter-library loans and librarians may not upload nature content on a large scale into their, or any other, institutional repository.

To the fullest extent permitted by law Nature Research makes no warranties, representations or guarantees to Users, either express or implied with respect to the nature content and all parties disclaim and waive any implied warranties or warranties imposed by law, including merchantability or fitness for any particular purpose.

Please note that these rights do not automatically extend to content, data or other material published by Nature Research that we license from third parties.

If you intend to distribute our content to a wider audience on a regular basis or in any other manner not expressly permitted by these Terms please contact us at

onlineservice@springernature.com